Neutron Scattering from a Poly(oxyethylene)−Poly(oxypropylene)−Poly(oxyethylene) Copolymer in Dilute Aqueous Solution under Shear Flow

Stephen M. King,*,† Richard K. Heenan,† Veronica M. Cloke,‡,§ and Clive Washington[||]

Large-Scale Structures Group, ISIS Facility, Rutherford Appleton Laboratory, Chilton, Didcot OX11 0QX, U.K., Department of Chemical Engineering, Imperial College, Prince Consort Road, London SW7 2BY, U.K., and Department of Pharmaceutical Sciences, University of Nottingham, University Park, Nottingham NG7 2RD, U.K.

Received May 5, 1997; Revised Manuscript Received July 29, 1997[⊗]

ABSTRACT: A small-angle neutron scattering study of the temperature dependence of the micellar structure has been performed on a 1% w/w aqueous solution of the poly(oxyethylene)−poly(oxypropylene)−poly(oxyethylene) (POE−POP−POE) block copolymer Synperonic P-85 using a Poiseuille-geometry shear flow apparatus. The system is characterized by two transition temperatures. The first is the critical micellization temperature at 24 °C. This marks the lower boundary of a spherical, later more ellipsoidal, micellar phase. The next transition is at 62 °C, above which the micelles may be adequately modeled as rigid rods. By 73 °C, rods with diameters of 10−12 nm and lengths of almost 400 nm have been attained. This micellar growth takes place without any appreciable increase in the radius of the micelles. The response of the rodlike micelles to the presence of the shear flow field is also reported.

Introduction

ABA-type triblock copolymers of poly(oxyethylene) (POE) A blocks and poly(oxypropylene) (POP) B blocks are water-soluble, nonionic, macromolecular surfactants with many and diverse applications. In this work we have concentrated on just one copolymer, that commonly designated Synperonic (or Pluronic) P-85. This has the approximate composition $(POE)_{26}-(POP)_{39}-(POE)_{26}$. The colloidal behavior of P-85 in water is comprehensively detailed by refs 1−20 and the references contained therein. The phase diagram may be found in ref 16.

Recent small-angle neutron scattering[10] (SANS) and dynamic light scattering[15] (DLS) studies have shown that at temperatures close to 70 °C there is a change in the shape of the copolymer micelles from spherelike to rodlike. We have also used SANS to study the temperature dependence of the micellar structure but with a significant difference. In order to probe the regime of the rodlike micelles in more detail, we have utilized a Poiseuille-geometry shear flow apparatus designed for in-situ use on a SANS instrument. To the best of our knowledge, the work reported here is the first to use the combination of neutron scattering and shear flow to investigate a Pluronic system not in a lyotropic liquid crystalline phase. These techniques have, however, provided much valuable information about related systems such as, for example, the short-chain, nonionic, ethylene glycol monoether surfactants like $C_{16}E_6$.

The advantages of using shear flow in conjunction with SANS or light scattering for the study of anisometric particles are well established.[21−23] If the micelles can be made to align in a shear field, then the orientational averaging effect normally conferred on the static scattering pattern by the thermal motion of the micelles is potentially removed. Analysis of the resulting anisotropic scattering pattern can then provide information on the micellar dimensions parallel and perpendicular to the direction of flow. By combining data from this type of experiment with that from rheological measurements, it is also possible to gain an insight into the dynamic system as, for example, might be encountered in the industrial arena.

Experimental Section

Sample. Deuterium oxide, D_2O, 99.8 atom % D, was purchased from both Aldrich Chemical Co. Ltd. and K. & K. Greef and was used as supplied.

Synperonic P-85 was donated by ICI Surfactants, Middlesbrough, U.K. As supplied, the copolymer is an opalescent paste with a melting point of 40 °C and a bulk density, *d*, of 1.03 g cm^{-3} (manufacturers data), though independent determinations of the density have given values around 1.15 g cm^{-3}.[18,20] Since the commercial material has been reported to contain small amounts of the diblock and other impurities, it was purified before use as detailed below.

P-85 has the formula $HO(C_2H_4O)_a(C_3H_6O)_b(C_2H_4O)_aH$ where *a* and *b* have been reported to have values in the ranges 25−27 and 38−40, respectively. This gives the copolymer a molecular weight between 4400 and 4700. Thus, approximately 50% (by weight) of the segments are POP.

Published critical micellization concentration data for P-85 span some 4 orders of magnitude from 0.0004 to 4% w/w,[4,13,18] and the whole issue has therefore been the subject of intensive study in recent years. The present consensus[18] seems to indicate a critical micellization concentration of around 0.04% w/w at 25 °C. In this work we have used 1% w/w solutions, a compromise between the need to ensure that micelles would be present, a desire to minimize intermicellar interactions, and the time needed to achieve adequate statistics in the available neutron beamtime. At this concentration we show that the system may also be approximated to a Newtonian fluid, except at the highest temperatures we have studied (>70 °C).

The P-85 solutions were prepared by allowing an appropriate amount of the purified copolymer to dissolve in D_2O (and H_2O in the case of the turbidimetry measurements) at room temperature over a period of several days in sealed volumetric flasks.

* To whom all correspondence should be addressed.
† ISIS Facility.
‡ Imperial College.
§ Now at Esso Petroleum Co. Ltd., Esso Refinery, Fawley, Southampton SO45 1TX, U.K.
|| University of Nottingham.
⊗ Abstract published in *Advance ACS Abstracts,* September 15, 1997.

S0024-9297(97)00623-2 CCC: $14.00

Purification of Sample. The P-85 was purified using an adaptation of the column chromatographic method of Bentley et al.[24] This removes a range of ionic impurities by ion exchange, and low molecular weight materials by adsorption on silica. In this work, P-85 (5 g) was dissolved in D_2O (to 50 cm^3) and stirred for 30 min with Amberlite MB-1 mixed bed resin (2 g). The resin was then filtered off and 2 g of silica gel (60-120 mesh, BDH Ltd.) added to the solution. After a further 30 min of stirring the silica gel was removed by centrifugation (15 min at 2000*g*).

Turbidimetry. An aliquot of polymer solution was placed in a cylindrical glass cell 2 cm in diameter. The cell was equipped with a magnetic flea and heated from below by a stirrer−hot plate at approximately 3 °C/min. Temperatures were recorded by a digital thermometer with a thermocouple probe in a stainless steel sheath (RS Components, Catalogue No. 650-419) to an accuracy of ±0.5 °C. The solution was illuminated with the direct beam from a 10 mW helium−neon laser (Melles Griot) operating at a wavelength of 633 nm, and the scattering at 90° was collected by a sheathed polymer optical fiber (RS Components) approximately 2 cm from the sample cell. The other end of the optical fiber was fed to a photomultiplier tube (EMI Model 9813B, at 1.2 kV), the output of which was displayed on a digital storage oscilloscope (Tektronix Model 2211).

The cloud points of the solutions were determined to be 85 °C in H_2O and 82 °C in D_2O. The value for H_2O agrees well with published data,[3,16,20] which range from 83 to 87 °C, though, interestingly, where we see a small drop in the cloud point in D_2O, workers studying the C_iE_j surfactants see a small increase.[25] A similar isotope effect was evident at the sphere-to-rod transition temperature, which was determined to be 64−65 °C in H_2O and 62−63 °C in D_2O. These values are up to 5 °C lower than those reported previously[10,15,16] but are consistent with the SANS data we report here.

Viscometry. The rheological properties of the system were studied using a Deer Rheometer (Integrated Petronic Instruments, London, U.K.). This is a constant stress concentric cylinder instrument of Searle geometry (rotating inner cylinder). An inner cylinder diameter of 14 mm was used with a gap of 0.5 mm. Temperature control to ±1 °C was provided by an external circulating fluid bath. The instrument was calibrated with D_2O. All of the viscosities reported in this paper are relative to the viscosity of D_2O at the indicated temperature. The maximum reliable shear rate attainable in this instrument was 2500 s^{-1}.

Small-Angle Neutron Scattering. SANS measurements were performed on the LOQ diffractometer[26] at the ISIS Spallation Neutron Source, Oxfordshire, U.K.[27] This is a fixed-geometry, time-of-flight (TOF), instrument equipped with position-sensitive "area" detectors and which utilizes neutrons with wavelengths between 0.2 and 1.0 nm to provide a continuous Q-range of approximately 0.08−16.0 nm^{-1}. The quantity Q

$$Q = (4\pi/\lambda)\sin(\theta/2) \qquad (1)$$

is the modulus of the scattering vector, the resultant between the incident and scattered wavevectors, where λ is the neutron wavelength and θ is the scattering angle. The wavelength resolution is effectively $\Delta\lambda/\lambda = 0.04$. The incident neutron beam was collimated to a diameter of $2r = 8$ mm.

The principal advantage of using a TOF instrument like LOQ, compared to a reactor-based (fixed wavelength) instrument, is that all of the Q range is accessible in a single measurement; there is no need to combine data sets covering different Q ranges. Such an instrument is therefore ideally suited to the study of systems where a range of length scales are involved or where model-fitting of the data is anticipated.

The calculated scattering length density, ρ, of each component follows: POE ($d = 1.13$ g cm^{-3}), $+0.637 \times 10^{10}$; POP ($d = 1.00$ g cm^{-3}), $+0.343 \times 10^{10}$; H_2O ($d = 0.99$ g cm^{-3}), -0.560×10^{10}; and D_2O ($d = 1.10$ g cm^{-3}), $+6.355 \times 10^{10}$ cm^{-2}.

For static (zero shear) measurements the polymer solution was placed in 1 or 2 mm path length, UV-spectrophotometry grade, synthetic quartz cuvettes (Hellma (England) Ltd.) with PTFE stoppers. Sample volumes were between 0.2 and 1.0 cm^{-3} depending on the path length and geometry of the cells. The cells were mounted in aluminum holders on top of an enclosed, computer-controlled, sample changer. Temperature control was achieved through a combination of electrical cartridge heaters in the sample holders and a thermostatically-controlled circulating bath pumping fluid through the base of the sample changer. Under these conditions the temperature stability was ±0.5 °C and experimental measuring times were between 10 and 20 min.

For SANS measurements under Poiseuille shear the polymer solution was contained in the apparatus described below with the beam center on the horizontal midline of the flow cell.

All scattering data were normalized for the sample transmission and incident wavelength distribution, background-corrected using an appropriate quartz cell filled with D_2O (this also removed the inherent instrumental background from vacuum windows, etc.), and corrected for the linearity and efficiency of the detector response using the instrument-specific software package.[28] The resulting one-dimensional scattering data (differential scattering cross-section, $d\Sigma/d\Omega(Q)$, versus Q) was in absolute units (cm^{-1}). Calibration of the absolute scale was achieved using the scattering from a well-characterized partially-deuterated poly(styrene) blend standard sample.[29]

The static scattering patterns were all isotropic, but some of the scattering patterns obtained under shear exhibited azimuthal anisotropy and so the raw data were processed slightly differently in these cases. While the isotropic data were radially integrated over all azimuthal angles (the usual practice), the anisotropic data were only radially integrated within 60° sectors, one about the direction of flow, the other about the mutually orthogonal direction on the detector. Thus for each anisotropic scattering pattern *two* one-dimensional data sets were generated. During the analysis these were model-fitted *simultaneously*.

To characterize the changes taking place in the system, we have fitted the SANS data to different analytical models for the scattering, using in-house software based around least-squares and Marquardt global minimization algorithms.[30] The models describe the scattering cross-section in terms of *P(Q)*, the shape or form factor, and *S(Q)*, the intermolecular structure factor, in the scattering function

$$\frac{d\Sigma}{d\Omega}(Q) = A(\phi_p)(\rho_p - \rho_{solvent})^2 P(Q)\, S(Q) + \text{background} \qquad (2)$$

where A, which is linearly dependent on the concentration, was parametrized as a scale factor in the fitting process. How closely the apparent concentration, ϕ_p^{app}, obtained from the model-fitting, matches the real concentration, ϕ_p, may be taken as an indication of how physically realistic a given model is. The other parameters in the model were the contrast, $(\rho_p - \rho_{solvent})^2$, the physical dimensions (from the *P(Q)* term), and a Q-independent background. At the solution concentration we have used in this work, we were able to adequately model the data without including intermolecular interactions. Including an *S(Q)* function does give a small improvement in the quality of the fit, but it must be remembered that this has been achieved through the inclusion of additional parameters.

Poiseuille Shear Flow Apparatus. This apparatus has been described in detail elsewhere.[31] Below we give a brief description in order that the experimental results may be better understood.

The apparatus forms a closed recirculating system, comprising a synthetic quartz flow cell (Optiglass Ltd.), a gear pump (for pulseless flow), and a glass in-line flow meter. Temperature control is achieved with electrical heaters and two K-type thermocouples. One thermocouple is situated just before the entrance to the flow cell and the other is approximately halfway around the circuit. The temperature difference across the apparatus is generally no more than ±2 °C. We have demonstrated an operational temperature range for the apparatus of 10−125 °C.

Inside the flow cell the fluid passes through a rectangular channel 1 mm in path length and 20 × 50 mm in elevation.

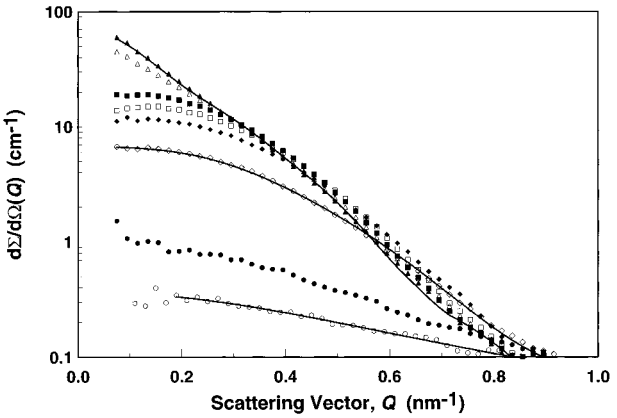

Figure 1. Variation with temperature of the SANS from a 1% w/w solution of Synperonic P-85 in D_2O. $\dot{\gamma} = 0$ s^{-1}. Key: (○) 13 °C; (●) 24 °C; (◊) 33 °C; (♦) 42 °C; (□) 51 °C; (■) 60 °C; (△) 64 °C; (▲) 73 °C. The solid lines are fits of the Debye form factor to the data at 13 °C, the polydisperse spherical form factor to the data at 33 °C, and eq 5 (the solid rod form factor) to the data at 73 °C.

At the two ends of the channel the quartz has been carefully machined so that it tapers to the internal diameter of the interconnecting tubing ($^5/_{32}$ in. 4 mm) in such a way as to minimize the formation of back eddies and vortices, though it is likely that a fluid will be subjected to some extensional flow in these regions.

In the case of Poiseuille shear flow, characterized by a parabolic shear rate profile, the *area average* shear rate across the channel (in the direction perpendicular to the incoming neutron beam), $\dot{\gamma}$, is directly related to the volumetric flow rate, F, through[31]

$$\dot{\gamma} = \frac{2F}{wh^2}\frac{(m+2)}{(m+1)} \tag{3}$$

where w is the width of the channel walls, h is their separation, and m is a dimensionless quantity relating the viscosity and consistency of the fluid to the shear rate.[32] For a Newtonian fluid, $m = 1$, and thus eq 3 leads to the following simple expression for the Poiseuille flow cell described above

$$\dot{\gamma}\ (\mathrm{s}^{-1}) = 2500F\ [\mathrm{L\ min}^{-1}] \tag{4}$$

The pump is capable of delivering flow rates of up to 1.8 L min^{-1} if the apparatus is filled with water, corresponding to a maximum shear rate of *circa* 5000 s^{-1}.

Results and Discussion

The discussion section of this paper is structured as follows. First, we briefly reiterate the phase behavior in this system, in the absence of a shear flow field, based on observations from our own experimental data. This not only allows us to compare the behavior of our system with the published results of other groups (though these vary in solvent, concentration, and temperature range) but also provides the basis by which we can compare and contrast the behavior of the system under the influence of the shear flow field. We then discuss an approach by which the SANS from rodlike micelles subject to Poiseuille shear flow may be interpreted and modeled and then use this to provide detailed information about the size and growth of the rodlike micelles.

Static Measurements. Figure 1 shows how the SANS from a 1% w/w solution of P-85 in D_2O changes with temperature. It can be seen that the scattering changes markedly on two occasions; once between 24 and 33 °C and again between 60 and 64 °C. To characterize the changes in both size and shape that are taking place in the polymer solution as it is heated, these data have been fitted to three different expressions for the form factor $P(Q)$. These were[33,34] the Debye function for the scattering from a random coil polymer of z-average radius-of-gyration R_g (assuming a polymer polydispersity of $M_w/M_n \sim 1.15$), the function for a homogeneous solid sphere of radius R_s (assuming a Schultz particle size distribution of 20%; an arbitrary value that is perhaps an overestimate, particularly at the lower temperatures, but one based on our experience of similar systems and which also extended the applicability of this model to higher temperatures where, as we shall see, the micelles are less spherical[35]), and the function for the scattering from a homogeneous solid rod or cylinder of radius R_c and length $2H$ where the major axis is orientated at an angle β with respect to Q:

$$P(Q,R_c,H,\beta) = \int_0^{\pi/2} \frac{4\sin^2(QH\cos\beta)\,J_1{}^2(QR_c\sin\beta)}{(Q^2H^2\cos^2\beta)\,(Q^2R_c{}^2\sin^2\beta)}\sin\beta\,\mathrm{d}\beta \tag{5}$$

where J_1 is a first-order Bessel function of the first kind. We have not convoluted the rod form factor with a polydispersity function for reasons of complexity.

The results from the model-fitting analysis are presented in Table 1. Fits outside of a models range of validity have been bracketed. In each case only the contrast parameter was constrained at its known value, and for simplicity we have not allowed for the very small difference in contrast between the POE and POP blocks of the copolymer in the analysis of the static scattering data.

In addition, the apparent micellar aggregation number, N_{agg}, at each temperature was obtained by dividing the apparent molecular weight, M, derived from a Zimm plot of the scattering data (eq 6), by the known monomeric molecular weight of P-85. The results have been plotted as a function of temperature in Figure 2.

$$\frac{K}{\frac{\mathrm{d}\Sigma}{\mathrm{d}\Omega}(Q)} \approx \frac{1}{M}\left(1 + \frac{Q^2R^2}{3}\right) \quad \text{where}$$

$$K = \frac{\phi_P(\rho_p - \rho_{solvent})^2}{N_A\mathrm{d}^2} \tag{6}$$

At temperatures ≤17 °C the Debye model provides an adequate description of the scattering and indicates the presence of "scattering bodies" with an $R_g \sim 3.4$ nm. The apparent molecular weight at these temperatures is a little higher than the monomeric value ($N_{agg} \sim 1.1$−1.4), and so it seems likely that we are observing transient associations of at least two polymer molecules.

Above 21 °C the Debye model is no longer realistic. The reason for this can be seen in Figure 2; there is a sharp jump in N_{agg} between 24 and 25 °C that we identify as the critical micellization temperature of this particular system. Our range for the critical micellization temperature can be compared with literature determinations, *measured in* H_2O, of 29[13,17] to 33.5 °C,[16] though on the evidence already presented we would expect to see a lower critical micellization temperature in our system due to isotope effects. Interestingly, neither the Debye nor spherical form factors fit the SANS data particularly well between 24 and 33 °C, suggesting that the spherical micellar architecture is

Table 1. Physical Dimensions and Apparent Concentrations Derived from Model-Fitting of the SANS Data from a 1% w/w Solution of Synperonic P-85 at Different Temperatures[a]

			Gaussian coil model[a]		sphere model[a]		solid rod model[a]		hydrated corona rod model		
T (°C)	$\dot{\gamma}$ (s^{-1})	Γ	R_g	ϕ_p^{app}	$\langle R_s \rangle$	ϕ_p^{app}	$R_c \times 2H$	ϕ_p^{app}	$R_c \times 2H$	t	ϕ_p^{app}
13	0	0	3.1 ± 0.2	1.2							
17	0	0	3.7 ± 0.2	1.4							
21	0	0	3.8 ± 0.2	1.7							
24	0	0	(4.3 ± 0.1)	(3.8)	(3.8 ± 0.1)	(0.1)					
33	0	0	(5.2 ± 1.5)	(29.5)	4.4 ± 0.1	0.4					
42	0	0			4.8 ± 0.1	0.7					
51	0	0			5.2 ± 0.1	0.8	4.8 × 10.9	0.5			
51	1300	0.0006					4.5 × 11.8	0.6	5.2 × 11.4	2.3	0.9
60	0	0			5.4 ± 0.1	0.8	5.0 × 11.7	0.6			
60	500	0.0003					4.7 × 12.4	0.6	5.5 × 12.0	2.5	0.9
65	2750	0.0095					4.9 × 22.3	0.6	5.7 × 22.3	2.6	1.0
73	0	0					5.1 × 35.0	0.7			
73	800	4.2					4.9 × 404	0.6	5.6 × 396	2.5	0.9
73[b]	800	4.8							6.3 × 412	3.3	2.2
73[c]	800	4.9							5.5 × 421	2.2	1.7
75	1900	2.5							6.0 × 229	2.7	1.3
77	800	3.8					5.0 × 389	0.6	5.9 × 378	2.6	0.8
81	700	3.4							6.5 × 375	2.9	1.1

[a] $N_w^{POE} = 3$ and $N_w^{POP} = 0$ except for (a) where $N_w^{POE} = 0$, (b) where $N_w^{POE} = 6$, and (c) where $N_w^{POP} = 1$. Dimensions are given in nm; apparent concentrations are given in % w/w. Radii in the rod models are ±0.1 nm. Lengths are ±2.5%.

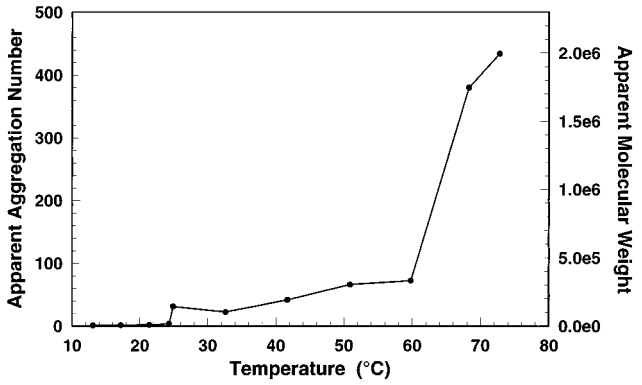

Figure 2. Variation with temperature of the apparent aggregation number and molecular weight, derived from the static SANS data, for a 1% w/w solution of Synperonic P-85 in D_2O.

not properly established until perhaps around 40 °C, at which point the micelles have a radius of about 5 nm. The average overall radii of the spherical micelles then show a small increase with increasing temperature.

Between 50 and 60 °C the micelles are probably ellipsoidal; the SANS data can be modeled almost equally as well by the polydisperse spherical model as by the solid rod model, the latter suggesting axial ratios for the ellipsoids of only slightly greater than 1:1.

Above 65 °C only the rod model adequately describes the data. A small degree of temperature-induced one-dimensional growth of the micelles then takes place, ultimately increasing the axial ratio to about 1:3 at 73 °C. The radii of the rods remains almost constant, at values very similar to the radii of the spherical micelles below the sphere-to-rod transition temperature. Our models cannot tell us, however, if, above 63 °C, there is a homogeneous population of rodlike micelles or a mixture of spherical and rodlike micelles. We defer any further discussion of the rod dimensions to the next section.

Shear Measurements. Below the transition temperature the scattering is isotropic. Above the transition temperature the scattering remains isotropic in the absence of the shear flow field, but once the field is applied, two "lobes" of scattering develop. These lobes, perpendicular to both the plane and direction of flow, are a characteristic signature of the presence of aligned *anisometric* micelles. Analysis of the scattering along the direction of the lobes, Q_{perp}, provides information across the diameter of the micelles, while the scattering in the direction at 90° to this, Q_{para}, provides information along the length of the micelles.

The advent of the scattering lobes, and their overall appearance, reveal a lot about the system. The inherent random thermal motion of the micelles may be characterized by a rotational diffusion coefficient, D_{rot}. For there to be any alignment whatsoever, $\dot{\gamma} > D_{rot}$. (The dimensionless ratio of these two numbers is sometimes called the Peclét number, a quantity we shall denote as Γ.) For a rod $D_{rot} \propto H^{-3}$, and so, from an experimental viewpoint, the less rodlike a rod becomes, the harder it is to align it. Furthermore, and all other factors being unchanged, the greater the degree of "necking" in the Q_{para} direction, the greater the degree of alignment and the greater the axial ratio of the micelles. Using the appropriate expressions,[21a,36] it is quite straightforward to show that for a rod of radius 5 nm to be aligned in the system we have studied, it must have a length $2H \geq 200$ nm. This is of course a considerably larger estimate of the length of the rodlike micelles than was extracted from the model fits to the *static* scattering data and highlights an inherent problem with the study of the quiescent system.

Equation 5 is not, however, a valid model for the scattering obtained under shear flow because in addition to β three other angles are necessary to describe an aligned system; two polar angles, θ and ϕ, to specify the orientation of a rodlike micelle in the experimental coordinate system, and the angle between Q and the direction of flow, ψ.

An expression for the form factor for rods aligned by *Couette shear flow* (where there is a linear shear rate profile) has been presented by Hayter and Penfold.[21] This has the form

$$P(Q,R_c,H,\Gamma,\theta,\phi,\psi) = \int_0^{2\pi}\int_0^{\pi} \Omega(\theta,\phi,\Gamma)\,[P_{rod}(Q,R_c,H,\beta_+) + P_{rod}(Q,R_c,H,\beta_-)] \sin\theta \, d\theta \, d\phi \quad (7)$$

where $P_{rod}(Q,R_c,H,\beta)$ is the form factor in eq 5,

$$\cos\beta_{\pm} = \sin\theta\cos\phi\cos\psi \pm \cos\theta\sin\psi \qquad (8)$$

and $\Omega(\theta,\phi,\Gamma)$ is a probability distribution function describing the likely orientation of a rod for a particular value of Γ and is given by[37]

$$\Omega(\theta,\phi,\Gamma) = \frac{[1-\cos(2\phi_0)][1+\sin^2(\theta)\cos(2\phi_0)]^{3/2}}{4\pi[1-\sin^2(\theta)\cos(2\phi_0)\cos 2(\phi-\phi_0)]^2}$$

$$\text{where} \qquad 2\phi_0 = \arctan\left(\frac{8}{\Gamma}\right) \qquad (9)$$

Equation 9 is valid for any type of shear flow provided that $\dot{\gamma}$ is constant. Thus, strictly speaking, for application to Poiseuille shear flow, $\Omega(\theta,\phi,\Gamma)$ should be integrated over the range of shear rates present within that volume element of the flow channel illuminated by the neutron beam.[38] Although this range of shear rates is calculable,[31b] for computational expediency we have chosen to use eq 9 in the form given above, but with a single shear rate averaged over the area of the neutron beam instead. This is expected to be a reasonable approximation providing $m \geq 1$ and $2r < w$.

Another problem with applying the Hayter−Penfold expression for $P(Q,R_c,H,\Gamma,\theta,\varphi,\psi)$ to the case of Poiseuille shear flow lies with the bracketed term in eq 7. Unlike our apparatus, in Couette (concentric cylinder) shear apparatus the neutron beam passes through the sample twice, but compared to the entrance region, the direction of flow in the exit region is reversed. This is the origin of the two P_{rod} terms. Unfortunately, it is not clear how the bracketed term should be modified for the case of Poiseuille shear flow, though a number of possible modifications do seem readily apparent. For this reason we have taken a rather more pragmatic approach and have elected to use eq 7 as it stands. This is undoubtedly a much coarser approximation than that we have used for the probability distribution function, but one that appears not to be quite as bad as one might think. To test this approximation we have run identical samples under both Poiseuille and Couette shear flow. The findings are discussed in the Appendix to this paper.

We have simultaneously fitted eq 2 to the $d\Sigma/d\Omega(Q_{perp})$ and $d\Sigma/d\Omega(Q_{para})$ components of the shear-aligned SANS data utilizing eq 7. As in the previous section, we have ignored the $S(Q)$ term and have not convoluted eq 7 with a size polydispersity function. The shear rate $\dot{\gamma}$ was constrained to its experimental value, leaving a scale factor, R_c, H, Γ, and a Q-independent background as the variable parameters. The contrast parameter was also constrained at its calculated value, but this time allowance was made for the difference in contrast between the POE and POP blocks of the copolymer. This was because the aligned data are of higher resolution.

The contrast difference between the two blocks was also enhanced by the fact that POE coordinates water molecules (in this case molecules of D_2O, which raised the effective scattering length density of the POE segments). Reported values for the degree of hydration, N_w^{POE}, vary from about 1.5 to 6 per POE segment.[39,40] In our analysis we have used $N_w^{POE} = 3$, which can probably be described as the modal value, and which corresponds to a corona containing about 56% D_2O (by volume). A natural consequence of incorporating this contrast difference is that our model was then also able to provide estimates of the thickness of the POE corona, t, surrounding the predominantly POP core of the rodlike micelles.

If one makes the assumption that solvent molecules only penetrate the corona, then from simple geometric arguments it follows that the thickness of the corona is a constant fraction of the total radius of a micelle for a given degree of hydration, since

$$\frac{\text{volume}_{shell}}{\text{volume}_{rod}} = \frac{R_c^2 - (R_c - t)^2}{R_c^2} = \frac{2a(V_{POE} + N_w^{POE}V_{D_2O})}{b(V_{POP} + N_w^{POP}V_{D_2O}) + 2a(V_{POE} + N_w^{POE}V_{D_2O})} \qquad (10)$$

To calculate the third equality, we have used the molar volumes of the components, V (where $V_{POE} = 42.77$, $V_{POP} = 56.39$, and $V_{D_2O} = 18.08$ cm^3 mol^{-1}). For $N_w^{POE} = 3$ this yields $t = 0.45R_c$, but ranges from $0.36R_c$ for $N_w^{POE} = 1$ to $0.53R_c$ for $N_w^{POE} = 6$. We note in passing that recent rheological and densitometric studies[41] provide strong evidence that the POP segments might also be coordinating 1 water molecule per segment. The effect of incorporating POP hydration into eq 10 (i.e., $N_w^{POE} > 0$) is to *reduce* the shell thickness calculated above by between 10 and 14% (the reduction diminishing as the ratio of POE-bound to POP-bound water increases).

The results from the model-fitting analysis are also shown in Table 1. The solid rod model is analogous to the rod model used to analyze the static SANS data (i.e., $N_w^{POE} = 0$, $t = 0$). Notice that allowing for the hydration of the corona has a small effect on the overall radii of the micelles but a negligible effect on their length, as might be expected from eq 10. It can also be seen that the model incorporating a hydrated corona actually fits the absolute intensities of the experimental data better than the solid rod model (the values of ϕ_p^{app} for the hydrated corona model allow for the coordinated water molecules). Furthermore, at temperatures above the sphere-to-rod transition temperature, the micellar lengths given in Table 1 are much more consistent with the rotational diffusion coefficient arguments outlined earlier. The greatest axial ratio that is obtained under shear is about 1:38. The data at 73 °C were also fitted to models with different values of N_w^{POE} and N_w^{POP}, but as can be seen from the table, the concentration scaling of these models was inferior.

The only other published data on the dimensions of the rodlike micelles is that of Schillen et al.[15] (which also appears in the slightly more recent review article by Almgren et al.[2]) and was obtained by analysis of the rotational component of the relaxation time distribution function from polarized dynamic light scattering experiments. Unlike our approach, this was only able to yield an estimate of a rod length for a *specified* micellar radius. At 75 °C they obtained micellar lengths between 185 and 200 nm for $R_c = 5$ nm. For larger radii, or for temperatures above or below 75 °C, the rodlike micelles were predicted to be shorter. These results are therefore consistent with our own, even to the point that we observe a maximum in a graph of the average anisotropy ratio[42] (related to the axial ratio of the micelles) versus temperature (at constant shear rate) at about 77 °C; see Figure 3. This peak is not unexpected. As we have already discussed, on the low temperature side the rodlike micelles are still evolving and are therefore influenced by the presence of the shear flow field to differing extents. On the high temperature side, approaching the cloud point, the POE segments are being

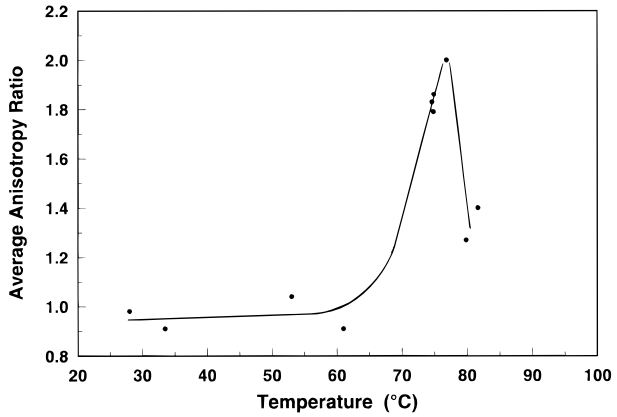

Figure 3. Variation of the average anisotropy ratio with temperature for a 1% w/w solution of Synperonic P-85 in D_2O at an area average shear rate of $\dot{\gamma} = 600\ s^{-1}$. The continuous line is a guide for the eye.

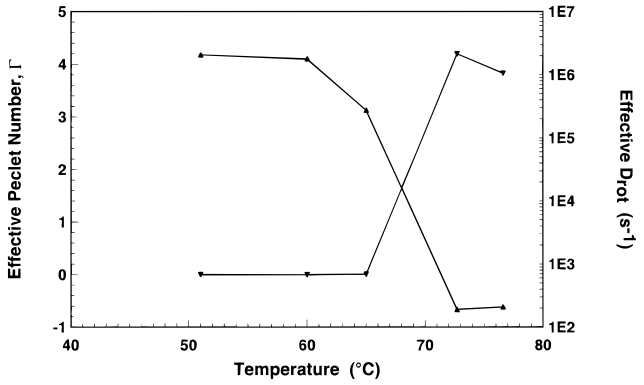

Figure 4. Variation of the effective Peclét number (▼) and effective rotational diffusional coefficient (▲) with temperature for a 1% w/w solution of Synperonic P-85 in D_2O.

progressively dehydrated. Again, by analogy with the C_iE_j surfactants this could lead to a reduction in the length of the rodlike micelles, driven by changes in the surface area-to-volume ratio of the POE segments in each micelle corona. There is some evidence of such an effect in Table 1, where it can be seen that raising the temperature from 73 to 77 °C has reduced the rod lengths by almost 20 nm. Further increases in temperature then appear to swell the rods rather than bring about any significant additional shortening. This of course also serves to reduce the axial ratio, and therefore the degree of alignment, but it is unlikely that the preceding discussion is a complete description of the behavior of the rods so close to the cloud point.

Since the model-fitting procedure incorporated Γ as a refining parameter, this can be used to calculate the effective rotational diffusion coefficient, D_{rot}. The variation of both quantities with temperature in the vicinity of the sphere-to-rod transition is shown in Figure 4. As the micelles elongate and align with the flow, the Peclét number increases and rotational motion diminishes. Even allowing for a 2−3° deuterium isotope effect, the values of D_{rot} recovered from the SANS data are about 1 order of magnitude lower than those obtained by Schillen et al.,[15] though this is no doubt a reflection of the difference in rod lengths as measured by the two different techniques.

Perhaps more intriguing is the effect of shear rate on the average anisotropy ratio (at constant temperature). This is shown at 75 °C in Figure 5. Up to a shear rate of approximately $\dot{\gamma} = 1000\ s^{-1}$, the anisotropy ratio is effectively constant, implying that there is little change

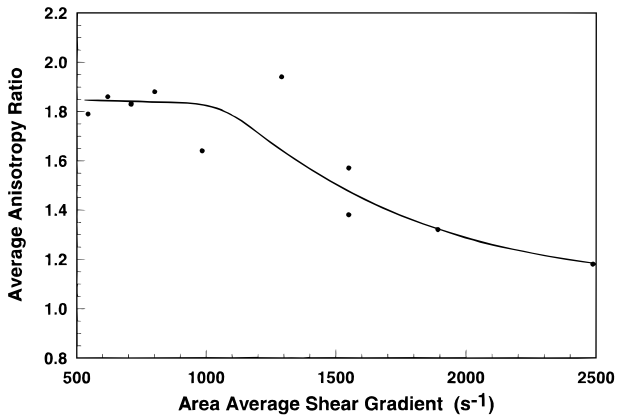

Figure 5. Variation of the average anisotropy ratio with area average shear rate for a 1% w/w solution of Synperonic P-85 in D_2O at a temperature of 75 °C. The continuous line is a guide for the eye.

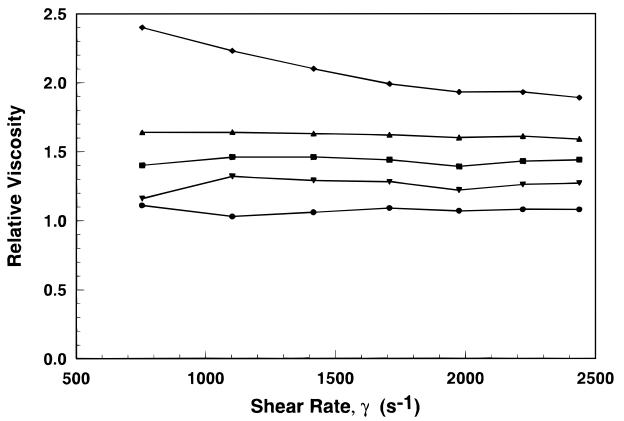

Figure 6. Relative viscosity of a 1% w/w solution of Synperonic P-85 in D_2O at selected temperatures, as measured in a Searle geometry rheometer. Each data set corresponds to a different micellar geometry, with increasing temperature; *n*-mers → spheres → ellipsoids → short rods → long rods. Key: (●) 22 °C; (▼) 42 °C; (■) 53 °C; (▲) 63 °C; (♦) 74 °C.

in the axial ratio of the rodlike micelles. Thereafter, the anisotropy ratio gradually decreases with increasing shear rate, signaling that the alignment of the micelles is decreasing, until at $\dot{\gamma} = 2500\ s^{-1}$ it has decreased from almost 2 to just under 1.2. The most likely explanation for this loss of alignment is that the rodlike micelles are getting shorter, as seems to be supported by the data in Table 1. If one compares the data for 73 and 77 °C with the data for 75 °C, where the shear rate has been doubled, it can be seen that the rod length has decreased from *circa* 390 nm at 800 s^{-1} to 230 nm at 1900 s^{-1}.

The anisotropy would diminish if the micelles were exhibiting a reduced effective axial ratio, perhaps through interactions with other micelles, but this does not appear to be supported by the shear rate dependence of the relative viscosity.[43] This is shown for selected temperatures in Figure 6. Below the sphere-to-rod transition temperature it can be seen that the relative viscosity is essentially independent of the shear rate; i.e., the solution is Newtonian ($m = 1$). Above the transition temperature there is evidence of shear-thinning behavior. While this is common in systems of anisometric particles, it is a characteristic of fewer intermicellar interactions, not more of them. We note in passing that similar behavior has recently been reported in, albeit rather more concentrated, aqueous solutions of the homologue Synperonic F-127 ($a = 100$, $b = 65$).[44] Furthermore, the dependence of $\dot{\gamma}$ on m is

quite small, scaling approximately as $3:(2 + (1/m))$; thus, if m doubled, a rather unlikely increase it must be said, $\dot{\gamma}$ would only drop to 83% of its value when $m = 1$.

We do not believe that the behavior shown in Figure 5 is due to the onset of turbulent flow since at this temperature the Reynolds number, Re, for the system, given by

$$\mathrm{Re} = \frac{D_{\mathrm{solution}} F}{w \eta_{D_2O}\, \eta_{\mathrm{rel}}} \tag{11}$$

where η_{rel} is the viscosity of the solution relative to that of D_2O, $\eta_{D_2O,}$ is less than 1200 even at the maximum flow rate depicted, and flow is considered laminar for Re < 2000 and turbulent for Re > 4000. Furthermore, all SANS measurements were performed at a point along the flow channel where any nonlaminar flow would have been either minimal or absent.[45]

Concluding Remarks

A SANS study of the dilute solution phase behavior of the POE−POP−POE block copolymer Synperonic P-85 as a function of temperature was conducted. Measurements were made on the quiescent system, and on the system subject to a Poiseuille shear flow field.

By model-fitting the scattering data to a range of simple functions for the size and shape of the polymer molecules and their aggregates, we have been able to corroborate previous reports of how the solution structure evolves with increasing temperature; Gaussian coils → loose aggregates of a few polymer molecules → spherical micelles → ellipsoidal or short rodlike micelles → long rodlike micelles.

The shear flow alignment of micelles in the rod phase has allowed us to make realistic and detailed determinations of the micellar dimensions that were not possible in the randomly oriented system. Our data suggest that the micelles are roughly twice as long, *circa* 400 nm at 73 °C, as has been previously reported. Even so, intermicellar interactions do not appear to be significant at the polymer concentration studied (1% w/w). The other dimensions are broadly comparable with literature data, overall micellar radii of *circa* 5.5 nm of which the outer 2.5 nm is a well-solvated corona of POE segments.

Though the model we have used to analyze the aligned data was developed for a different type of shear flow (Couette), we have demonstrated in the Appendix to this paper that to a reasonable approximation the equations are still applicable.

One remaining question concerns the flexibility of the rodlike micelles, since the analysis we have used assumes the rods to be relatively rigid. The opposite extreme is that of the Kratky−Porod wormlike micelle, characterized by a persistence length, l. If $2H > l > R_c$, then for such a model one would expect to see a change in the functional form of the SANS at low-Q from almost Q^{-1} (the dependence of a rigid rod; the exponent is only minus one for an infinitely-thin worm) to Q^{-2} (the dependence of a flexible Debye Gaussian coil).[46] We do not see any definite evidence of this crossover in the Q range we have examined, and this leads us to conclude that l is relatively large (very crudely l may be of the order of π/minimum accessible $Q \approx 39$ nm). Thus the micelles are more rigid than they are flexible.

We are currently using this combination of SANS and shear flow to examine the phase behavior of related POE/POP block copolymers in dilute solution.

Table 2. Physical Dimensions and Apparent Concentrations Derived from Model-Fitting of the Shear-Aligned SANS Data from a 1% w/w Solution of $C_{16}E_6$ at 30 °C[a]

shear flow	$\dot{\gamma}$ (s^{-1})	anisotropy ratio	$R_c \times 2H$	ϕ_p^{app}	ϕ_p^{actual}
Couette[39]	5000	not stated	3.3 × 400	0.5	0.6
Couette	5275	7.7	3.1 × 333	1.6	1.2
Couette	475	2.5	2.9 × 557	1.4	1.1
Poiseuille	5000	2.3	2.7 × 250	1.9	1.2

[a] $N_w^{POE} = 3$ and $N_w^{C16} = 0$. Dimensions are given in nm; apparent concentrations are given in % w/w. Radii are ±0.1 nm. Lengths are ±2.5%.

Acknowledgment. The authors would like to thank the U.K. Engineering and Physical Sciences Research Council and ISIS for the provision of neutron beamtime, ICI Surfactants for donating the Synperonic P-85, Helen Hermes for providing an additional pair of hands during the experiments, and Julia Higgins and Jeff Penfold for their interest in this work. V.M.C. would like to thank Shell Research for the award of a postgraduate studentship. S.M.K. would also like to acknowledge the contribution to the data analysis provided by Karin Shmueli during a vacation studentship.

Appendix

Here we outline the results of a comparative study of the effects of Poiseuille and Couette shear flow on the same sample under the same conditions using SANS.

Since the Couette shear apparatus available to us had an upper temperature limit, imposed by its method of construction, below the P-85 sphere-to-rod transition temperature we have instead used a 1% w/w solution of the nonionic surfactant hexaethylene glycol monohexadecyl ether (or 6 cetyl ether), commonly denoted as $C_{16}E_6$, at a temperature of 30 °C. This system has the benefit of having been widely studied, and in particular, data are available on the dimensions of the rodlike micelles formed by this surfactant under these conditions.[39]

Two approaches have been compared. In the first, the area average shear rate for the Poiseuille shear apparatus was set as close to the shear rate used with the Couette shear apparatus (*circa* 5000 s^{-1}) as possible. In the second, because our previous work[31] showed that the degree of alignment observed under Poiseuille shear flow was not as great as that achieved under Couette shear flow, the shear rate for the Couette apparatus was adjusted until the anisotropy ratio of the scattering[42] approximately matched that achieved in the Poiseuille shear apparatus at an area average shear rate of 5000 s^{-1} (an anisotropy ratio of *circa* 2.3).

The results of model-fitting eqs 7−9 to the SANS data from this system are compared in Table 2.

The differences in the micellar radii are not statistically significant, but the variations in the micellar lengths are (one standard deviation being no more than ±10 nm). That said, the two data sets obtained under Couette shear flow at a nominal shear rate of 5000 s^{-1} show quite good agreement, though the literature data, obtained at a slightly lower shear rate and with a completely different sample, suggest the presence of somewhat longer micelles. It is of course possible that as the shear rate is raised, hydrodynamic forces break down the very long rodlike micelles, as appears to be the case in the P-85/D_2O system.

The important point about these data is that the data obtained under Poiseuille shear flow correlate much better with the Couette data obtained at the *same shear*

rate than they do with the Couette data obtained at the same anisotropy ratio (same degree of alignment). This is despite a factor of 3 difference in the anisotropy ratios. Thus the fact that the lengths of the micelles appear underestimated in the case of Poiseuille shear flow is just as likely to be a consequence of the poorer degree of alignment, reducing the sensitivity of the experiment to the lengths and flexibilities of the rods, as a consequence of our application of a model developed for Couette shear flow. We therefore submit that to a reasonable level of approximation Poiseuille shear flow data may be interpreted using eqs 7−9 with the provisos outlined in the main text.

It will also be observed that, compared to the P-85 data, the concentration scaling of these data are rather less satisfactory. This is because at 1% w/w there is a much larger contribution to the scattering from the $S(Q)$ term in this system that cannot be treated within the framework of this model. The literature data in the table, however, are at a lower concentration and so are less affected by this contribution.

References and Notes

(1) Chu, B. *Langmuir* **1995**, *11*, 414.
(2) Almgren, M.; Brown, W.; Hvidt, S. *Colloid Polym. Sci.* **1995**, *273*, 2.
(3) Physical Properties of the Pluronic Polyols, Data Sheet F-3025, BASF Wyandotte Corp., Parsippany, NJ.
(4) Schmolka, I. R.; Raymond, A. J. *J. Am. Oil Chem. Soc.* **1965**, *42*, 1088.
(5) Prasad, K. N.; Luong, T. T.; Florence, A. T.; Paris, J.; Vaution, K.; Seiller, M.; Puisieux, F. *J. Colloid Interface Sci.* **1979**, *69*, 225.
(6) Vadnere, M.; Amidon, G.; Lindenbaum, S.; Haslam, J. L. *Int. J. Pharm.* **1984**, *22*, 207.
(7) Killman, E.; Maier, H.; Baker, J. A. *Colloid Surf.* **1988**, *31*, 51.
(8) Brown, W.; Schillen, K.; Almgren, M.; Hvidt, S.; Bahadur, P. *J. Phys. Chem.* **1991**, *95*, 1850.
(9) Mortensen, K. *Europhys. Lett.* **1992**, *19*, 599.
(10) Mortensen, K.; Pedersen, J. S. *Macromolecules* **1993**, *26*, 805.
(11) Mortensen, K.; Brown, W. *Macromolecules* **1993**, *26*, 4128.
(12) Linse, P. *Macromolecules* **1993**, *26*, 4437.
(13) Alexandridis, P.; Holzwarth, J. F.; Hatton, A. T. *Macromolecules* **1994**, *27*, 2414.
(14) Wanka, G.; Hoffmann, H.; Ulbricht, W. *Macromolecules* **1994**, *27*, 4145.
(15) Schillen, K.; Brown, W.; Johnsen, R. M. *Macromolecules* **1994**, *27*, 4825.
(16) Glatter, O.; Scherf, G.; Schillen, K.; Brown, W. *Macromolecules* **1994**, *27*, 6046.
(17) Nivaggioli, T.; Alexandridis, P.; Hatton, T. A.; Yekta, A.; Winnik, M. A. *Langmuir* **1995**, *11*, 730.
(18) Kabanov, A. V.; Nazarova, I. R.; Astafieva, I. V.; Batrakova, E. V.; Alakhov, V. Yu.; Yaroslavov, A. A.; Kabanov, V. A. *Macromolecules* **1995**, *28*, 2303.
(19) Zhang, K.; Khan, A. *Macromolecules* **1995**, *28*, 3807.
(20) Meilleur, L.; Hardy, A.; Quirion, F. *Langmuir* **1996**, *12*, 4697.
(21) (a) Hayter, J. B.; Penfold, J. *J. Phys. Chem.* **1984**, *88*, 4589. (b) Cummins, P. G.; Staples, E.; Millen, B.; Penfold, J. *Meas. Sci. Technol.* **1990**, *1*, 179. (c) Penfold, J.; Staples, E.; Cummins, P. G. *Adv. Colloid Interface Sci.* **1991**, *34*, 451.
(22) Lindner, P.; Oberthur, R. C. *Rev. Phys. Appl.* **1984**, *19*, 759; *Colloid Polym. Sci.* **1985**, *263*, 443; **1988**, *266*, 886.
(23) (a) Cummins, P. G.; Staples, E.; Penfold, J.; Heenan, R. K. *Langmuir* **1989**, *5*, 1195. (b) Cummins, P. G.; Penfold, J.; Staples, E. *Langmuir* **1992**, *8*, 31.
(24) Bentley, P. K.; Davis, S. S.; Johnson, O. L.; Lowe, K. C.; Washington, C. *J. Pharm. Pharmacol.* **1989**, *41*, 661.
(25) Staples, E. Private communication.
(26) (a) Heenan, R. K.; Penfold, J.; King, S. M. *J. Appl. Crystallogr.*, in press. (b) King, S. M.; Heenan, R. K. The LOQ Instrument Handbook. Rutherford Appleton Laboratory Report RAL TR-96-036; RAL: Didcot, Oxon., U.K., 1996.
(27) See http://www.isis.rl.ac.uk/index.htm.
(28) (a) King, S. M.; Heenan, R. K. Using COLETTE. Rutherford Appleton Laboratory Report RAL 95-005; RAL: Didcot, Oxon., U.K., 1995. (b) Heenan, R. K.; King, S. M.; Osborn, R. I.; Stanley, H. B., COLETTE Users Guide. Rutherford Appleton Laboratory Report RAL 89−128; RAL: Didcot, Oxon., U.K., 1989.
(29) Wignall, G. D.; Bates, F. S. *J. Appl. Crystallogr.* **1987**, *20*, 28.
(30) (a) Heenan, R. K. FISH Data Analysis Program. Rutherford Appleton Laboratory Report RAL 89-129; RAL: Didcot, Oxon., U.K., 1989. (b) Osborn, R., FRILLS: an Interactive Least-Squares Fitting Package. Rutherford Appleton Laboratory Report RAL 91−011; RAL: Didcot, Oxon., U.K., 1991.
(31) (a) Higgins, J. S; Cloke, V. M.; Phoon, C. L.; Richardson, S. M.; King, S. M.; Done, R.; Cooper, T. E. *Rev. Sci. Instrum.* **1996**, *67*, 3158. (b) Cloke, V. M. Ph.D. Thesis, Imperial College, London, 1996.
(32) When a fluid is nonNewtonian: if it shear-thickens, then $m < 1$; if it shear-thins, then $m > 1$. In the shear-thinning case, as m increases the parabolic shear rate profile characteristic of Poiseuille flow becomes broader and shallower. This has the effect of reducing the range of fluid velocities distributed across the flow channel, effectively making the shear rate profile more linear. Under these conditions the area average shear rate approximates to the velocity average shear rate.
(33) See: Higgins, J. S.; Benoît, H. C. *Polymers and Neutron Scattering*; Oxford University Press: Oxford, U.K., 1994.
(34) Livsey, I. *J. Chem. Soc., Faraday Trans. 2* **1987**, *83*, 1445.
(35) An explicit form factor for *spherical* block copolymer micelles, resolving both the "core" and "shell" dimensions, has recently been proposed: Pedersen, J. S.; Gerstenberg, M. C. *Macromolecules* **1996**, *29*, 1363. We note that these authors utilized a core radius polydispersity of 13%.
(36) Broersma, S. *J. Chem. Phys.* **1960**, *32*, 1626; **1981**, *74*, 6989.
(37) Bird, R. B.; Hassager, O.; Armstrong, R. C.; Curtiss, C. F. *Dynamics of Polymeric Liquids*; Wiley: New York, 1977; Vol. 2.
(38) Penfold, J. Private communication.
(39) Cummins, P. G.; Hayter, J. B.; Penfold, J.; Staples, E. *Chem. Phys. Lett.* **1987**, *138*, 436.
(40) (a) Molyneux, P. *Water. A Comprehensive Treatise*; Plenum Press: New York, 1975; Vol. 4. (b) Eagland, D.; Crowther, N. J.; Butler, C. J. *Polymer* **1993**, *34*, 2804. (c) Hey, M. J.; Ilett, S. M.; Davidson, G. *J. Chem. Soc., Faraday Trans.* **1995**, *91*, 3897. (d) Bieze, T. W. N.; Barnes, A. C.; Huige, C. J. M.; Enderby, J. E.; Leyte, J.C. *J. Phys. Chem.* **1994**, *98*, 6568.
(41) Crowther, N. J.; Eagland, D. *J. Chem. Soc., Faraday Trans.* **1996**, *92*, 1859.
(42) We define the anisotropy ratio of the scattering to be the average of the ratio $(d\Sigma/d\Omega\ (Q))_{perp}/(d\Sigma/d\Omega\ (Q))_{para}$ obtained at the (arbitrary) Q values 0.075, 0.295, and 0.595 nm^{-1}. This is, however, a rather coarse definition and can lead to anisotropy ratios in an isotropic system that are not quite unity.
(43) These data were measured in the Searle rheometer where there is a single defining shear rate. This is *not* the case with the Poiseuille shear flow apparatus; there, the area average shear rate is a convenient means of representing a range of shear rates, and so care should be exercised in making direct comparisons between the different pieces of apparatus. For example, at an area average shear rate of 1000 s^{-1}, a Newtonian fluid in the Poiseuille shear flow apparatus will experience shear rates ranging from 0 s^{-1} at the center of the channel to 2000 s^{-1} at the walls. Similarly, at 2000 s^{-1} the range is 0−4000 s^{-1}. As m increases, this range becomes less exaggerated.
(44) Prud'homme, R. K.; Wu, G. W.; Schneider, D. K. *Langmuir* **1996**, *12*, 4651.
(45) The distance after which a fluid passing between two parallel plates is in fully developed laminar flow, the entrance length, L_e, is given by $L_e = ch\mathrm{Re}$ where c is a dimensionless experimental constant (see ref 31) of the order 0.01−0.05. Thus we calculate $L_e \sim 35$ mm. The channel in the flow cell was 50 mm in length.
(46) Schurtenberger, P.; Magid, L. J.; King, S. M.; Lindner, P. *J. Phys. Chem.* **1991**, *95*, 4173.

MA9706236